Proceedings Paper:
Dedeoglu, S. and Konstantopoulos, G.C. (2021) Avoiding circulating current via current-limiting control in AC microgrids with parallel three-phase inverters. In: IECON 2021 – 47th Annual Conference of the IEEE Industrial Electronics Society. IECON 2021 – 47th Annual Conference of the IEEE Industrial Electronics Society, 13-16 Oct 2021, Toronto, ON, Canada (virtual). Institute of Electrical and Electronics Engineers. ISBN: 9781665402569. ISSN: 1553-572X. EISSN: 2577-1647.

https://doi.org/10.1109/iecon48115.2021.9589420

Avoiding Circulating Current via Current-Limiting Control in AC Microgrids with Parallel Three-Phase Inverters

Seyfullah Dedeoglu
Dept. of Automatic Control and Systems Engineering
The University of Sheffield
Sheffield, S1 3JD, UK
sdedeoglu1@sheffield.ac.uk

George C. Konstantopoulos
Dept. of Electrical and Computer Engineering
University of Patras
26504 Rio, Patras, Greece
g.konstantopoulos@ece.upatras.gr

***Abstract*—In this paper, an AC microgrid consisting of paralleled three-phase inverters is investigated and a nonlinear droop controller is proposed. The purpose of the proposed controller is twofold: i) to avoid circulating power among the paralleled inverters and ii) to guarantee a current-limiting property at each inverter in both stand-alone and grid-connected modes, as well as during the transition between them. Contrary to the existing methods that utilize saturation blocks to limit the reference current value, the proposed controller limits the instantaneous value of the current even after extreme faults, i.e., short circuits in both grid-connected and stand-alone cases. Moreover, after incorporating the proposed controller dynamics into the system, the entire microgrid small-signal stability analysis is investigated. In order to validate the effectiveness of proposed controller, a microgrid, which includes three parallel three-phase inverters, is being tested via Matlab/Simulink software and extensive simulation results are provided.**

***Index Terms*—Nonlinear droop control, current limitation, circulating power, DC-link voltage control, stand-alone state, grid-connected state, parallel inverter operation, stability analysis.**

I. Introduction

Since it was originally introduced almost two decades ago, the microgrid concept has gained significant amount of attention due to its critical roles in the integration of renewable energy sources (RESs) into the grid [1]. Microgrids are considered as the essential components of the future power system due to their flexible control algorithms, environmental benefits, higher energy efficiencies, and seamless performance in both grid-connected (GC) and stand-alone (SA) applications [2]–[4]. Besides, as microgrids consist of various distributed generation (DG) units, and those units are connected to the grid via power electronic inverters (PEIs), proper control design for PEIs is required to ensure their seamless and reliable operations [5], [6].

Parallel operation of PEIs is preferred in microgrid applications, as the semiconductor components used in the PEIs have limited power ratings [7]. Although parallel PEI operation has the advantage to avoid overloading individual inverters by achieving power and load sharing via droop control [6]–[8], it can lead to undesired circulating power [9] and current [10] flows, especially in the GC to SA or SA to GC transitions and short circuit faults, between different inverter units. Droop control has been extensively adopted for load and power sharing in PEI applications, since it uses only local measurements without requiring external communication links [11], [12]. Due to their simple logic and implementation, many droop control algorithms, such as traditional $P \sim \omega$ and $Q \sim V$ droop, virtual impedance-based droop, adaptive and robust droop [11], universal droop [13], and their improved versions [14] have been proposed in the last decade. However, droop method has an inherent inability to accurately share the load and power in parallel inverter applications in case of different line parameters without a control algorithm switch.

Furthermore, ensuring the system stability in both GC and SA operations, and smooth mode transitions are two important issues for a reliable microgrid operation, which includes several parallel PEIs. Generally, those issues can be achieved via various compensation methods, such as virtual impedance, droop coefficient, and control algorithm changes [15], [16]. However, the mentioned methods may lead to unacceptable voltage, frequency and current fluctuations [17], which can damage the inverters, activate the protection relays, and eventually cause to instability.

In order to guarantee fail-safe operation and avoid transient instability phenomenon under large system faults, such as short circuits, in renewable energy or microgrid applications, every inverter in the system should be equipped with current-limiting algorithms [18], [19]. To overcome this critical issue, reference current limitation via saturated PI controllers [20] and virtual impedance-based algorithms [21] are being commonly used. However, both methods can lead to latch-up and wind-up problems, and eventually system instability [22], especially when PEI-based DGs are combined with conventional generators within the microgrid. Besides, undesired circulating power between parallel inverters can lead to component overheating, reduced efficiency, instability [10], and DC-link voltage increase [23]. This issue is examined for SA mode parallel

This work is supported by EPSRC under Grants No EP/S001107/1 and EP/S031863/1, and under Grant 81359 from the Research Committee of the University of Patras via "C. CARATHEODORY" program.

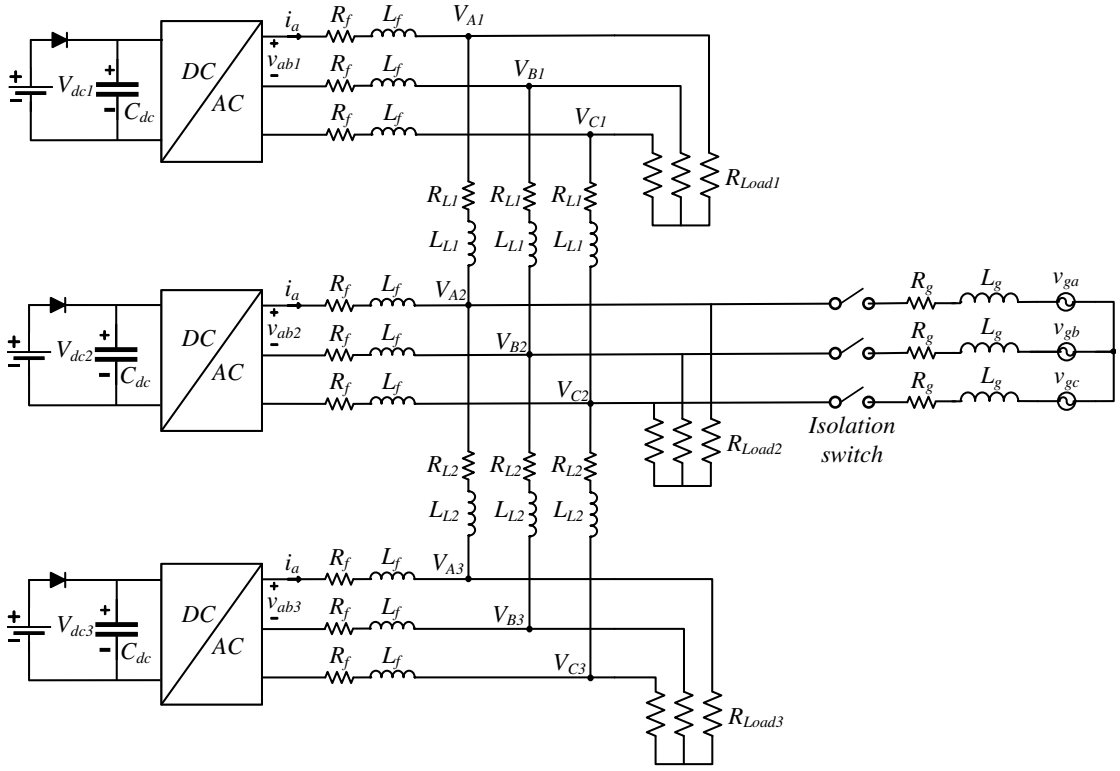

Fig. 1. The microgrid system under consideration.

inverters in [10] via feeder impedance compensation and in [23] using proportional-derivative (PD) DC-link voltage controllers. Recently, a bounded integral controller (BIC) has been proposed and used to limit the system current of parallel inverters in SA mode [24]. However, GC operation, and SA to GC or GC to SA transitions for parallel inverters have not been examined. An improved version of BIC has been proposed as state-limiting (sl) PI controller in [25] and applied to three-phase GC inverters [26]. Nevertheless, the performance of this controller for parallel inverters in SA or GC mode has not been investigated yet.

To this end, in this paper, both the current limitation and circulating power issues are being handled at the same time by integrating the universal droop control dynamics into the sl-PI controller and using a proportional DC-link controller, respectively. The proposed method can achieve current limitation and maintains the DC-link voltage under the given limit at all times including SA to GC and GC to SA transitions, and short circuits in both SA and GC modes, in parallel three-phase inverter applications. Since the proposed method does not require saturation blocks or control algorithm change in its implementation, the integration wind-up and latch-up problems are inherently solved. For a simple implementation, the controller dynamics are designed to align the local inverter current with d axis as in [26] instead of common approaches, which align the inverter voltage with the d axis [20]. Moreover, the small-signal stability of entire closed-loop system equipped with the proposed controller is investigated. The effectiveness of the proposed method is verified via extensive simulation studies in Matlab/Simulink software.

II. Microgrid System Modeling

The system under consideration is a microgrid, which includes three parallel three-phase inverters connected to individual loads and a point of common coupling (PCC) via L filters and lines, as depicted in Fig. 1. The considered system topology is similar to [23], however, in this paper, the grid-side is also regarded to examine the GC operation and transitions. The filter parasitic resistance and inductance are described as R_f and L_f, while the line inductances and resistances between the inverters are shown as L_{L1}, L_{L2}, R_{L1}, R_{L2}, respectively. Individual resistive loads for each inverter are denoted as R_{Load1}, R_{Load2}, and R_{Load3}. The line between the PCC and main grid has a resistance R_g and an inductance L_g, while grid-side abc frame voltages are denoted as v_{ga}, v_{gb}, and v_{gc}, respectively. The DC side of the inverters includes a DC-source, a diode, and a capacitor (C_{dc}) as adopted in [3]. Common frame inverter voltages are given as V_{Ai}, V_{Bi}, and V_{Ci}, where i denotes the inverter number. Following the analysis from [27], the local frame inverter dq voltages are obtained as

$$\begin{bmatrix} V_{dli} \\ V_{qli} \end{bmatrix} = \begin{bmatrix} V_{Di}\cos\delta_i + V_{Qi}\sin\delta_i \\ -V_{Di}\sin\delta_i + V_{Qi}\cos\delta_i \end{bmatrix}, \tag{1}$$

where $\delta_i = \theta_i - \theta_{com}$ denotes the phase angle difference between the inverter and common point. Then, the dynamic equations for each inverter in the local dq frame are given as

$$L_f \frac{di_{di}}{dt} = -R_f i_{di} + \omega_i L_f i_{qi} - V_{dli} + V_{di} \tag{2}$$

$$L_f \frac{di_{qi}}{dt} = -R_f i_{qi} - \omega_i L_f i_{di} - V_{qli} + V_{qi} \tag{3}$$

where i_{di}, i_{qi} and V_{di}, V_{qi} represent the local dq frame inverter currents and voltages, while $\omega_i = \dot{\theta}_i$ is the angular frequency of the inverter. Hence, using (1) and local frame inverter currents, the inverter active and reactive power can be calculated as

$$\begin{aligned} P_i &= \frac{3}{2}\left[\cos\delta_i\left(V_{Di}i_{di} + V_{Qi}i_{qi}\right) + \sin\delta_i\left(V_{Qi}i_{di} - V_{Di}i_{qi}\right)\right] \\ Q_i &= \frac{3}{2}\left[\cos\delta_i\left(V_{Qi}i_{di} - V_{Di}i_{qi}\right) - \sin\delta_i\left(V_{Di}i_{di} + V_{Qi}i_{qi}\right)\right]. \end{aligned} \tag{4}$$

As can be seen from (4), the power equations include nonlinear terms. Therefore, any control effort including the widely accepted droop and PI controls will make the closed-loop system nonlinear. In that case, since the linear theory-based controllers may not guarantee the stable and reliable operation, especially under large system faults, i.e., short circuits and transitions, nonlinear theory-based controllers should be designed. To this end, in this paper, a nonlinear controller is proposed to guarantee the current-limiting property for each inverter at all times, including the large system faults, while also preventing the circulating power via the DC-link voltage control.

III. The Proposed Current-Limiting and DC-link Controllers

In this section, the design steps for the proposed controller are explained in detail. With the application of universal droop control, the current-limiting property is achieved by embedding $P \sim V$ droop equations into the nonlinear sl-PI controller and the circulating power issue is resolved with the integration of proportional DC-link controller into the $Q \sim -\omega$ droop equations. Local inverter current is aligned with the d axis for a simple implementation and closed-loop stability analysis as in [26], opposed to the common approaches [20], which align the inverter voltage with the d axis. Thus, the inverter side local dq frame voltages (before the filter) are designed as control inputs and take the form

$$V_{di} = V_{dli} + E_{maxi}\sin\sigma_i - r_{vi}i_{di} - \omega_i L_f i_{qi} \tag{5}$$

$$V_{qi} = V_{qli} - r_{vi}i_{qi} + \omega_i L_f i_{di} \tag{6}$$

where E_{maxi} and r_{vi} are the sl-PI controller parameters and denoted as virtual voltage and resistor, respectively. $\omega_i L_f i_{di}$ and $\omega_i L_f i_{qi}$ represent the decoupling terms, and σ_i is the sl-PI controller state, which is designed to include $P \sim V$ droop dynamics as below

$$\dot{\sigma_i} = \frac{c_i}{E_{maxi}}\left[(\sqrt{2}E^* - V_{maxi}) - n_i(P_i - P_{seti})\right]\cos\sigma_i \tag{7}$$

where c_i is the positive sl-PI controller gain. As proven in [25], if the initial condition of the controller state σ_i is selected as $\sigma_{i0} \in [-\frac{\pi}{2}, \frac{\pi}{2}]$, it is guaranteed that $\sigma_i(t) \in [-\frac{\pi}{2}, \frac{\pi}{2}]\ \forall t \geq 0$. Besides, contrary to traditional saturated PI controllers, the anti-windup property is inherently achieved with the proposed method, since the integration is decelerated near the maximum values, i.e., when $\sigma_i \to \pm\frac{\pi}{2}$, $\dot{\sigma_i} \to 0$.

Furthermore, the $P \sim V$ droop control is realized via regulating $(\sqrt{2}E^* - V_{maxi}) - n_i(P_i - P_{seti})$ to zero with the integration property of the sl-PI controller. In the droop expression, $\sqrt{2}E^*$ defines the nominal maximum common frame inverter voltage, V_{maxi} is the maximum common frame inverter voltage computed as $V_{maxi} = \sqrt{V_{Di}^2 + V_{Qi}^2}$, P_{seti} and n_i are the active power reference value and the active power droop coefficient, respectively.

The closed-loop system dynamics can be obtained by replacing the controller dynamics (5)-(6) into the system dynamics (2)-(3) as below

$$L_f\frac{di_{di}}{dt} = -(R_f + r_{vi})i_{di} + E_{maxi}\sin\sigma_i \tag{8}$$

$$L_f\frac{di_{qi}}{dt} = -(R_f + r_{vi})i_{qi} \tag{9}$$

As one can understand from (9), if initially $i_{qi}(0) = 0$, then $i_{qi}(t) = 0, \forall t \geq 0$. Thus, the analytic solution of (9) is obtained as $i_{qi}(t) = i_{qi}(0)e^{-\frac{(R_f + r_{vi})}{L_f}t}$. To this end, in order to guarantee the inverter current limitation, the sl-PI controller parameters can be chosen as $E_{maxi} = (r_{vi} + R_f)I_{di}^{max}$, where $I_{di}^{max} = \sqrt{2}I_{rmsi}^{max}$ and I_{rmsi}^{max} is the RMS current limit provided by the inverter producers. Particularly, d axis current i_{di} and the sl-PI controller state σ_i remain in the intervals $[-\sqrt{2}I_{rms}^{max}, \sqrt{2}I_{rms}^{max}]$ and $[-\frac{\pi}{2}, \frac{\pi}{2}]\ \forall t \geq 0$, respectively as proven in [28]. It is important to note that the current limitation is ensured for the original nonlinear system and independently of the large-signal system faults, including short circuits and transitions. It is suggested that the readers refer to [25] for the controller state-limiting property proven via nonlinear control theory. Since it is proven that q-axis inverter current is always zero, the power expressions (4) can be simplified as

$$\begin{aligned} P_i &= \frac{3}{2}\left(V_{Di}\cos\delta_i + V_{Qi}\sin\delta_i\right)i_{di} \\ Q_i &= \frac{3}{2}\left(V_{Qi}\cos\delta_i - V_{Di}\sin\delta_i\right)i_{di}. \end{aligned} \tag{10}$$

The angular frequency dynamics, which are necessary for abc to dq transformations are designed to include $Q \sim -\omega$ and proportional DC-link controller as

$$\omega_i = \omega^* + m_i\left(Q_i - Q_{seti} - k_{pi}(V_{dci} - V_{dcref})\right) \tag{11}$$

where ω^*, m_i, Q_{seti}, k_{pi}, and V_{dcref} are the nominal angular frequency, reactive power droop coefficient, reactive power set value, DC-link proportional controller gain, and reference DC-link voltage, respectively.

IV. Small-Signal Stability Analysis

Although the current-limiting property for the parallel-operated three-phase inverters is ensured in the previous section, the closed-loop stability of the entire system equipped with the proposed controller has not been investigated yet. Hence, in this section, the main focus is to examine the stability of i number of parallel inverters. Note that the line dynamics have not been considered in the stability analysis due to the page limitation, however, interested readers can refer to [27] for the entire system modeling. Since it is ensured

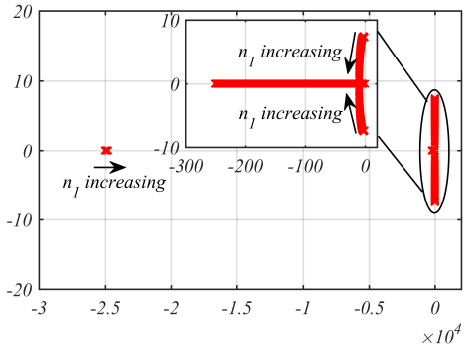

Fig. 2. Closed-loop eigenvalue spectrum of inverter 1 as a function of active power droop coefficient n_1 : $\frac{0.01\sqrt{2}E^*}{S_{max}} \leq n_1 \leq \frac{0.3\sqrt{2}E^*}{S_{max}}$

with the controller design that the q axis inverter current is zero at all times, (9) can be omitted from the closed-loop system analysis as it has been already investigated, separately. Considering (7)-(8), $\dot{\delta}_i = \omega_i - \omega_{com}$, and DC-link voltage dynamics in [3], the closed-loop state vector is constructed as $x_i = [i_{di}\ \sigma_i\ V_{dci}\ \delta_i]^T$. Root-locus analysis can be realized for the entire system by calculating the equilibrium points using (7), (8), and (11) as $x_{ei} = [i_{dei}\ \sigma_{ei}\ V_{dcei}\ \delta_{ei}]^T$, where $\sigma_{ei} \in (-\frac{\pi}{2}, \frac{\pi}{2})$, and by linearizing (7)-(8) and (10)-(11) and considering constant (or piecewise constant) PCC voltage V_{maxi}. Thus, the closed-loop system Jacobian matrix can be computed as (12) for every inverter i. As a result, the asymptotic stability of the given equilibrium point of the closed-loop system will be guaranteed, if all system eigenvalues are in left half plane.

$$J_i = \begin{bmatrix} -\frac{(r_{vi}+R_f)}{L_f} & \frac{E_{maxi}\cos\sigma_{ei}}{L_f} & 0 & 0 \\ -A_iB_i & 0 & 0 & -A_iC_ii_{dei} \\ \frac{3m_L}{C_{dc}}B_i & 0 & 0 & \frac{3m_Li_{dei}}{C_{dc}}C_i \\ \frac{3m_i}{2}C_i & 0 & -m_ik_p & -\frac{3m_ii_{dei}}{2}B_i \end{bmatrix}_{4i\times 4i} \quad (12)$$

where $A_i = \frac{3c_in_i\cos\sigma_{ei}}{2E_{maxi}}$, $B_i = (V_{Di}\cos\delta_{ei} + V_{Qi}\sin\delta_{ei})$, $C_i = (V_{Qi}\cos\delta_{ei} - V_{Di}\sin\delta_{ei})$, and m_L is the V_{dc} linearization coefficient and can be calculated as $\frac{1}{2V_{dcref}}$ as explained in [3].

In Fig. 2, the eigenvalue spectrum of closed-loop system for inverter 1 is demonstrated by changing the active power droop coefficient n_1 between 1% and 30%. The system and controller parameters used to plot the eigenvalue spectrum are given in Table I. As it is clear from Fig. 2, all eigenvalues are in left half plane. Similarly, one can test the eigenvalue spectrum of the other two inverters and realize that all eigenvalues are also located at the left half plane. Thus, the considered equilibrium point of the closed-loop system is asymptotically stable.

V. Simulation Results

In order to test the proposed current-limiting controller performance, a microgrid, which has three parallel connected three-phase inverters as in [23] and [27] is designed in the Matlab/Simulink software. Contrary to [23] and [27], which have examined only SA inverter operation and have not considered the current limitation issue, in this section, both the GC case and the SA to GC and GC to SA transitions are investigated. Simulated system and controller parameters are provided in Table I. The simulation starts in SA case (isolation switch is open) and the system is quickly regulated to the steady-state values as shown in Figs. 3 and 4 without any over-current problem as seen in Figs. 5 and 6. Between $t = 0.5s$ and $t = 0.6s$, 0.01Ω load is connected in parallel to R_{Load1} to test the SA case short circuit performance of the proposed controller. Although there is a transient peak in the reactive powers (Fig. 4), the frequencies (Fig. 7), and the maximum voltages (Fig. 9) at the fault recovery time instant, those do not affect the current-limiting property as illustrated in Figs. 5 and 6. Even after a large fault, the system responds very quickly and almost immediately reaches to the steady-state. At $t = 1s$, isolation switch is closed and grid connection is realized. As can be seen from Figs. 6, 7, and 9, no current, frequency, and voltage overshoot is induced and connection is achieved very smoothly. Between $t = 1.5s$ and $t = 1.7s$, a grid short circuit fault is applied to the system. Even in this extreme fault, the current-limiting property holds as shown in Figs. 5 and 6. Fig. 6 also justifies that the inverter current is aligned to d-axis ($i_{qi} = 0$) and this property is not influenced by the large system faults. DC voltage of the inverters is provided in Fig. 8. The transient changes in the DC-link voltages are also acceptable, since the circuit components can tolerate small overshoots. At $t = 2.5s$, GC to SA transition is conducted, and all figures support that the transition is achieved smoothly without any over-current or voltage encounters. At $t = 3s$, the simulation ends. If one wants to check the steady-state values of active powers and voltages according to the $P \sim V$ droop equation, zoomed maximum voltage in Fig. 9 can be used as a reference. To this end, the effectiveness of proposed controller is demonstrated with extensive simulation studies under several different scenarios that include both normal and faulty conditions.

TABLE I
Simulated System and Controller Parameters

Parameters	Values	Parameters	Values	Parameters	Values
P_{set1}	20kW	P_{set2}	10kW	P_{set3}	6.5kW
Q_{set1}	0VAR	Q_{set2}	0VAR	Q_{set3}	0VAR
R_{Load1}	25Ω	R_{Load2}	20Ω	R_{Load3}	38Ω
L_f	2mH	R_f	0.1Ω	n	0.00104
m	1.047×10^{-4}	E^*	220V	f^*	50Hz
V_{dcref}	750V	R_1	0.23Ω	L_1	0.32mH
R_2	0.35Ω	L_2	1.85mH	k_p	30
C_{dc}	1.1mF	m_L	6.5×10^{-4}	c	50000
ω^*	$2\pi f^*$	r_v	50Ω	I_d^{max}	67.276A
R_g	0.5Ω	L_g	2.2mH	S_{max}	30kVA

VI. Conclusions

In this paper, a nonlinear droop controller is proposed for parallel operated three-phase inverters. The proposed method can limit the inverter current via the sl-PI controller and prevent circulating power via DC-link voltage control at all times, including short circuit in SA and GC cases, and transitions. The closed-loop stability is investigated using small-signal modeling and root-locus analysis of the system has been demonstrated. The proposed controller performance is verified through extensive simulation results.

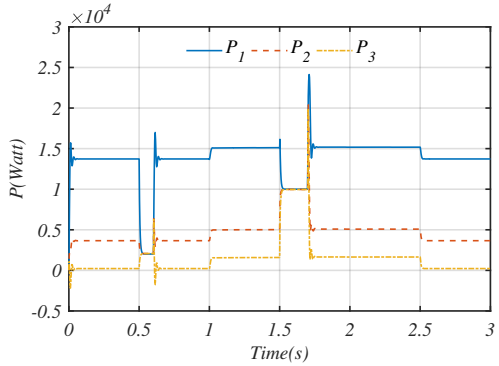

Fig. 3. Active power outputs of three parallel connected three-phase inverters

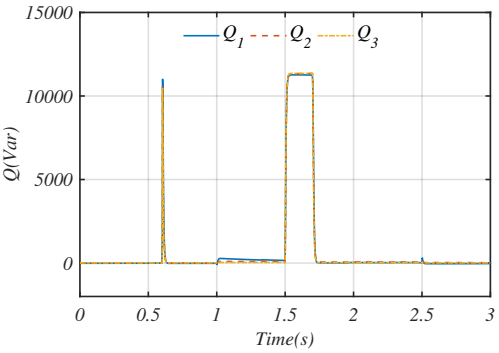

Fig. 4. Reactive power outputs of three parallel connected three-phase inverters

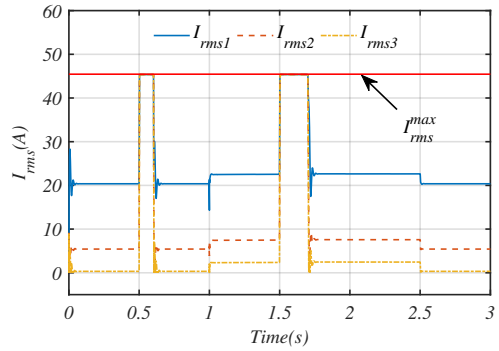

Fig. 5. RMS currents of three parallel connected three-phase inverters

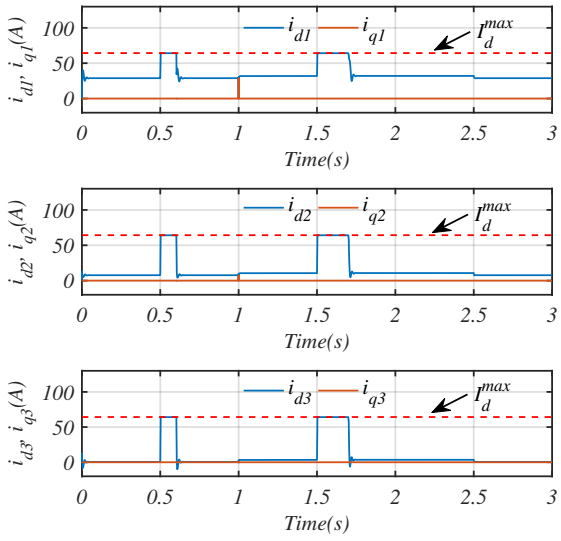

Fig. 6. *dq* frame currents of three parallel connected three-phase inverters

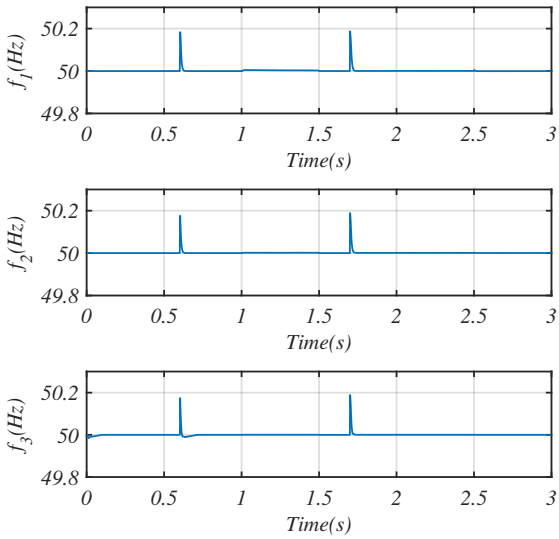

Fig. 7. Frequencies of three parallel connected three-phase inverters

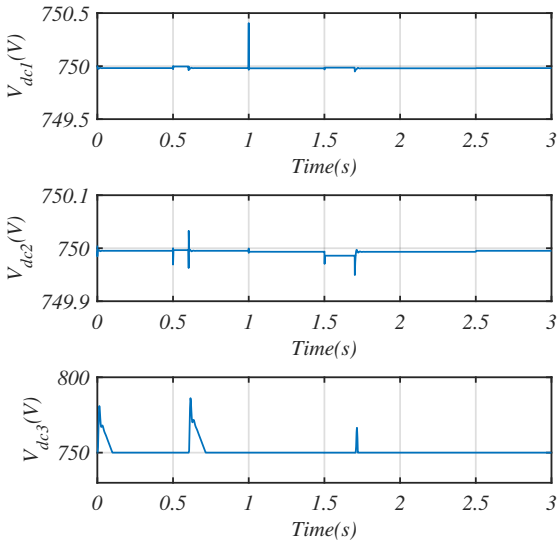

Fig. 8. DC voltages of three parallel connected three-phase inverters

REFERENCES

[1] A. Vasilakis, I. Zafeiratou, D. T. Lagos and N. D. Hatziargyriou, "The Evolution of Research in Microgrids Control," *IEEE Open Access Journal of Power and Energy*, vol. 7, pp. 331-343, 2020, doi: 10.1109/OAJPE.2020.3030348.

[2] D. E. Olivares et al., "Trends in Microgrid Control," *IEEE Transactions on Smart Grid*, vol. 5, no. 4, pp. 1905-1919, July 2014, doi: 10.1109/TSG.2013.2295514.

[3] W. R. Issa, M. A. Abusara and S. M. Sharkh, "Control of Transient Power During Unintentional Islanding of Microgrids," *IEEE Transactions on Power Electronics*, vol. 30, no. 8, pp. 4573-4584, Aug. 2015, doi: 10.1109/TPEL.2014.2359792.

[4] T. Morstyn, B. Hredzak and V. G. Agelidis, "Control Strategies for Microgrids With Distributed Energy Storage Systems: An Overview," *IEEE Transactions on Smart Grid*, vol. 9, no. 4, pp. 3652-3666, July 2018, doi: 10.1109/TSG.2016.2637958.

[5] T. Dragičević, S. Vazquez and P. Wheeler, "Advanced Control Methods for Power Converters in DG Systems and Microgrids," *IEEE Transactions on Industrial Electronics*, vol. 68, no. 7, pp. 5847-5862, July 2021, doi: 10.1109/TIE.2020.2994857.

[6] H. Han, X. Hou, J. Yang, J. Wu, M. Su and J. M. Guerrero, "Review of Power Sharing Control Strategies for Islanding Operation of AC

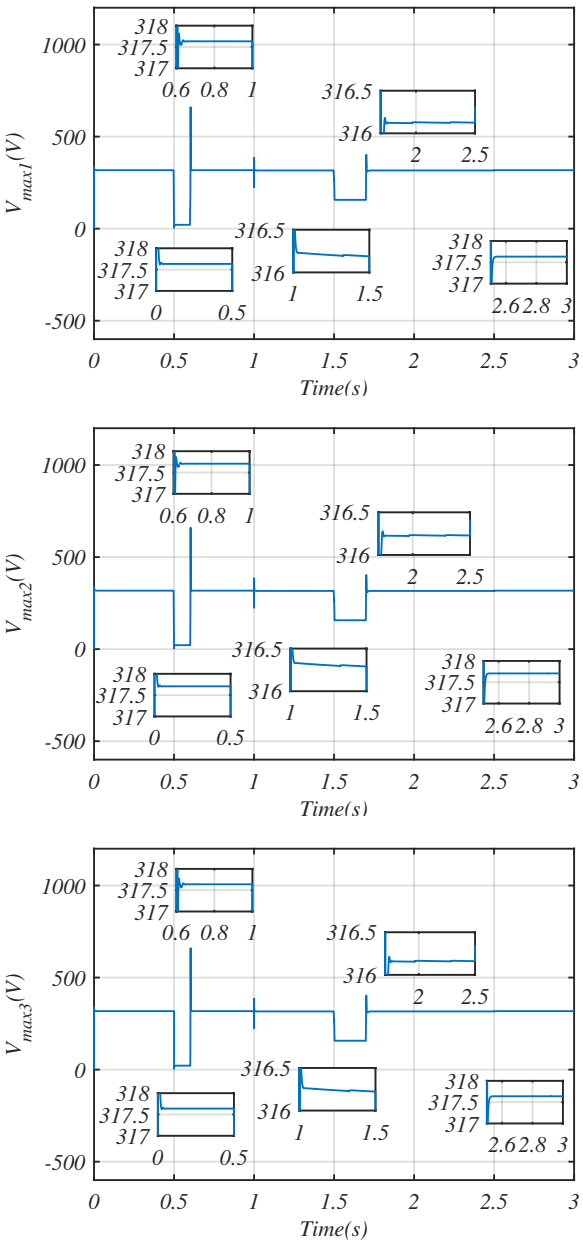

Fig. 9. The maximum value of the PCC voltages of three parallel connected three-phase inverters

Microgrids," *IEEE Transactions on Smart Grid*, vol. 7, no. 1, pp. 200-215, Jan. 2016, doi: 10.1109/TSG.2015.2434849.

[7] G. C. Konstantopoulos, Q. C. Zhong, B. Ren, and M. Krstic, "Bounded droop controller for parallel operation of inverters," *Automatica*, vol. 53, pp. 320–328, 2015, doi: 10.1016/j.automatica.2015.01.012.

[8] M. Farrokhabadi et al., "Microgrid Stability Definitions, Analysis, and Examples," *IEEE Transactions on Power Systems*, vol. 35, no. 1, pp. 13-29, Jan. 2020, doi: 10.1109/TPWRS.2019.2925703.

[9] W. R. Issa, A. H. E. Khateb, M. A. Abusara and T. K. Mallick, "Control Strategy for Uninterrupted Microgrid Mode Transfer During Unintentional Islanding Scenarios," *IEEE Transactions on Industrial Electronics*, vol. 65, no. 6, pp. 4831-4839, June 2018, doi: 10.1109/TIE.2017.2772199.

[10] M. Zhang, B. Song and J. Wang, "Circulating Current Control Strategy Based on Equivalent Feeder for Parallel Inverters in Islanded Microgrid," *IEEE Transactions on Power Systems*, vol. 34, no. 1, pp. 595-605, Jan. 2019, doi: 10.1109/TPWRS.2018.2867588.

[11] U. B. Tayab, M. A. Bin Roslan, L. J. Hwai, and M. Kashif, "A review of droop control techniques for microgrid," *Renewable and Sustainable Energy Reviews*, vol. 76, no. November 2016, pp. 717–727, 2017, doi: 10.1016/j.rser.2017.03.028.

[12] P. Prabhakaran, Y. Goyal and V. Agarwal, "Novel Nonlinear Droop Control Techniques to Overcome the Load Sharing and Voltage Regulation Issues in DC Microgrid," *IEEE Transactions on Power Electronics*, vol. 33, no. 5, pp. 4477-4487, May 2018, doi: 10.1109/TPEL.2017.2723045.

[13] Q. Zhong and Y. Zeng, "Universal Droop Control of Inverters With Different Types of Output Impedance," *IEEE Access*, vol. 4, pp. 702-712, 2016, doi: 10.1109/ACCESS.2016.2526616.

[14] B. M. Eid, N. A. Rahim, J. Selvaraj and A. H. El Khateb, "Control Methods and Objectives for Electronically Coupled Distributed Energy Resources in Microgrids: A Review," *IEEE Systems Journal*, vol. 10, no. 2, pp. 446-458, June 2016, doi: 10.1109/JSYST.2013.2296075.

[15] M. Ganjian-Aboukheili, M. Shahabi, Q. Shafiee and J. M. Guerrero, "Seamless Transition of Microgrids Operation From Grid-Connected to Islanded Mode," *IEEE Transactions on Smart Grid*, vol. 11, no. 3, pp. 2106-2114, May 2020, doi: 10.1109/TSG.2019.2947651.

[16] X. Meng, X. Liu, M. He, Z. Liu and J. Liu, "A Self-Adaptive Controller for Inverter With Seamless Transfer and Automatic Pre-Synchronization Capability," *IEEE Access*, vol. 8, pp. 105936-105949, 2020, doi: 10.1109/ACCESS.2020.3000268.

[17] M. N. Arafat, A. Elrayyah and Y. Sozer, "An Effective Smooth Transition Control Strategy Using Droop-Based Synchronization for Parallel Inverters," *IEEE Transactions on Industry Applications*, vol. 51, no. 3, pp. 2443-2454, May-June 2015, doi: 10.1109/TIA.2014.2369826.

[18] A. D. Paquette and D. M. Divan, "Virtual Impedance Current Limiting for Inverters in Microgrids With Synchronous Generators," *IEEE Transactions on Industry Applications*, vol. 51, no. 2, pp. 1630-1638, March-April 2015, doi: 10.1109/TIA.2014.2345877.

[19] L. Huang, H. Xin, Z. Wang, L. Zhang, K. Wu and J. Hu, "Transient Stability Analysis and Control Design of Droop-Controlled Voltage Source Converters Considering Current Limitation," *IEEE Transactions on Smart Grid*, vol. 10, no. 1, pp. 578-591, Jan. 2019, doi: 10.1109/TSG.2017.2749259.

[20] N. Pogaku, M. Prodanovic and T. C. Green, "Modeling, Analysis and Testing of Autonomous Operation of an Inverter-Based Microgrid," *IEEE Transactions on Power Electronics*, vol. 22, no. 2, pp. 613-625, March 2007, doi: 10.1109/TPEL.2006.890003.

[21] T. Qoria, F. Gruson, F. Colas, X. Kestelyn, and X. Guillaud, "Current limiting algorithms and transient stability analysis of grid-forming VSCs," *Electric Power System Research*, vol. 189, no. 691800, 2020, doi: 10.1016/j.epsr.2020.106726.

[22] N. Bottrell and T. C. Green, "Comparison of Current-Limiting Strategies During Fault Ride-Through of Inverters to Prevent Latch-Up and Wind-Up," *IEEE Transactions on Power Electronics*, vol. 29, no. 7, pp. 3786-3797, July 2014, doi: 10.1109/TPEL.2013.2279162.

[23] W. Issa, F. Al-Naemi, G. Konstantopoulos, S. Sharkh, and M. Abusara, "Stability analysis and control of a microgrid against circulating power between parallel inverters," *Energy Procedia*, vol. 157, pp. 1061–1070, 2019, doi: 10.1016/j.egypro.2018.11.273.

[24] G. C. Konstantopoulos, Q. C. Zhong, B. Ren, and M. Krstic, "Bounded droop controller for parallel operation of inverters," *Automatica*, vol. 53, pp. 320–328, 2015, doi: 10.1016/j.automatica.2015.01.012.

[25] G. C. Konstantopoulos and P. R. Baldivieso-Monasterios, "State-limiting PID controller for a class of nonlinear systems with constant uncertainties," *International Journal of Robust and Nonlinear Control*, vol. 30, no. 5, pp. 1770–1787, 2020, doi: 10.1002/rnc.4853.

[26] S. Dedeoglu, G. C. Konstantopoulos and A. G. Paspatis, "Grid-Supporting Three-Phase Inverters With Inherent Root Mean Square Current Limitation Under Balanced Grid Voltage Sags," *IEEE Transactions on Industrial Electronics*, vol. 68, no. 11, pp. 11379-11389, Nov. 2021, doi: 10.1109/TIE.2020.3034860.

[27] W. Issa, M. Abusara, S. Sharkh and T. Mallick, "A small signal model of an inverter-based microgrid including DC link voltages," *2015 17th European Conference on Power Electronics and Applications (EPE'15 ECCE-Europe)*, 2015, pp. 1-10, doi: 10.1109/EPE.2015.7309119.

[28] S. Dedeoglu and G. C. Konstantopoulos, "PLL-Less Three-Phase Droop-Controlled Inverter with Inherent Current-Limiting Property," *IECON 2019 - 45th Annual Conference of the IEEE Industrial Electronics Society*, 2019, pp. 4013-4018, doi: 10.1109/IECON.2019.8927219.